Automatic Self-Adaptive Local Voltage Control Under Limited Reactive Power

Rui Cheng, *Graduate Student Member, IEEE*, Naihao Shi, *Graduate Student Member, IEEE*,
Salish Maharjan, *Member, IEEE*, Zhaoyu Wang, *Senior Member, IEEE*

Abstract—**The increasing proliferation of distributed energy resources has posed new challenges to Volt/VAr control problems in distribution networks. To this end, this paper proposes an automatic self-adaptive local voltage control (ASALVC) by locally controlling VAr outputs of distributed energy resources. In this ASALVC strategy, each bus agent can locally and dynamically adjust its voltage droop function in accordance with time-varying system changes. The voltage droop function is associated with the bus-specific time-varying slope and intercept, which can be locally updated, merely based on local voltage measurements, without requiring communication. Stability, convergence, and optimality properties of this local voltage control are analytically established. In addition, the online implementation of ASALVC is further proposed to address the real-time system changes by adjusting VAr outputs of DERs online. Numerical test cases are performed to validate and demonstrate the effectiveness and superiority of ASALVC.**

Index Terms—**Volt/VAr control, local voltage control, distributed energy resource, distribution network.**

I. Introduction

Recent years have seen the increasing deployment and penetration of renewable energy resources, such as photovoltaic (PV) generators and wind, in power systems, which has led to over-/under-voltage problems due to the intermittent and volatile nature of renewable energy resources. Volt/VAr Control (VVC) strategies have shown a great capability to effectively resolve those voltage problems by controlling VAr outputs owing to the rapid development of inverter-based technologies for distributed energy resources (DERs) [1].

In the past decades, VVC strategies have been extensively and widely studied by researchers and practitioners. In general, it can be roughly divided into three main categories: centralized voltage control, distributed voltage control, and local voltage control.

Centralized voltage control ([2]-[4]) collects all the required information, such as network and load parameters, and then performs a central computation to solve the corresponding optimization and control problems. However, it usually suffers from large amounts of computation time, considerable communication overload, and privacy problems, hindering scalability.

Rather than collecting all problem parameters and performing a central calculation, distributed voltage control is computed by many agents that obtain certain parameters via coordinating communication [5]. According to the coordinating communication infrastructure, it can be further divided into hierarchical voltage control, where a central agent communicates with other agents in a hierarchical manner, and decentralized voltage control, where each agent communicates with its neighbors, but there is not a central agent. For example, hierarchical voltage control schemes, based on the Alternating Direction Method of Multipliers (ADMM) or projected Newton method, are applied to coordinate electric vehicle charging schedules, wind turbines, photovoltaic inverters in [6]-[9], respectively. Different network-constrained ADMM-based decentralized voltage control strategies are proposed in [10]-[11], relying on the communication between neighboring buses. Furthermore, some advanced online decentralized voltage control algorithms are developed in [12]-[14], where the real-time measurements are utilized to determine the control solution.

Compared to centralized voltage control and distributed voltage control, local voltage control typically only relies on local information without requiring communication, rendering itself a more practical and scalable implementation. The traditional droop control [15], [16], as advocated by IEEE 1547-2018 Standard [17], is one of the most common and popular local voltage control, which actively adjusts the VAr output as a function of voltage following a given 'Volt-VAr' piecewise linear characteristic. However, as shown in [16], the droop slope in the traditional droop control needs to be small enough to guarantee system stability. Moreover, the work [18] shows such a traditional droop control is not able to maintain a feasible voltage profile under certain circumstances. A modified 'delayed' droop control is proposed in [19] to improve the stability performance, but it is unclear how to determine the delay parameter to optimally balance the stability performance and convergence speed. The works [19]-[21] provide stability analysis, but all of them lack the optimality analysis and system-wide performance characterization resulting from the implementation of local voltage control. The works [22]-[23] formulate the local voltage control as optimization problems, exhibiting a better stability performance than the traditional and delayed droop control, where rigorous stability, convergence, and optimality analyses are provided. The studies [22]-[23] are both based on the (scaled/classical) gradient projection (GP) method, which can be regarded as one type of modified voltage droop control with a constant slope

and a time-varying intercept. However, the convergence rate of GP is relatively slow [24], [25], which is typically characterized by $O(1/k)$ (k is the iteration number), indicating relatively weak tracking capabilities to follow system variations. Moreover, the constant slope in [22]-[23] limits the diversity and flexibility of local voltage control to some degree.

To this end, this paper proposes an automatic self-adaptive local voltage control (ASALVC) to solve the VVC problem with the goal of mitigating the voltage deviations across distribution networks by locally controlling VAr outputs of DERs. This VVC problem is formulated as an optimization problem, which is first solved by a generalized fast gradient method (GFGM) [26], [27]. Interestingly, the GFGM iterations naturally decouple into *communication-free* local updates, which can be reinterpreted as our proposed local voltage control strategy, by properly choosing and designing parameters. Compared with existing studies, the main contributions of this study are as follows:

- This local voltage control is *automatic self-adaptive*, allowing each bus agent to locally and dynamically adjust its voltage droop function in accordance with time-varying system changes. This voltage droop function is associated with both *the bus-specific time-varying slope and intercept*, significantly increasing the diversity and flexibility of local voltage control.
- The time-varying slope and intercept are locally and intelligently updated by each bus agent merely based on its local voltage measurements without requiring communication, where *the closed-form expressions* of the bus-specific time-varying slope and intercept are analytically explored and presented.
- This automatic self-adaptive local voltage control exhibits *an accelerated convergence rate* both theoretically and practically, characterized by $O(1/k^2)$, in static scenarios, indicating *a better tracking capability* to follow time-varying changes in dynamic scenarios. *Stability, convergence, and optimality properties* of this self-adaptive local voltage control are first analytically established and then demonstrated by means of numerical test cases.

Remaining sections are organized as follows. The network modeling and problem statement are discussed in Section II. The GFGM-based VVC strategy is described in Section III. Section IV carefully explains the transition from the GFGM-based VVC strategy to this ASALVC by properly choosing and designing parameters. Both the offline and online implementation of this ASALVC are demonstrated in Section IV. Section V reports numerical test cases, and Section VI discusses ongoing and planned future studies.

II. NETWORK MODELING AND PROBLEM STATEMENT

Consider a radial distribution network with $N + 1$ buses. Let $\{0\} \bigcup \mathcal{N}$ denote the bus set, where $\mathcal{N} = \{1, 2, ..., N\}$. For each bus $j \in \mathcal{N}$, let V_i denote its voltage magnitude, p_i and q_i denote its real and reactive power injections. Let $b^p(j) \in \{0\} \cup \mathcal{N}$ denote the bus immediately preceding bus j along the radial distribution network, $\mathcal{L} = \{\ell_j = (i, j) | i = b^p(j), j \in \mathcal{N}\}$ denote the line segment set. For each line segment $(i, j) \in \mathcal{L}$,

TABLE I
NOMENCLATURE: OPERATOR

$< \boldsymbol{x}, \boldsymbol{y} >$	It denotes $\boldsymbol{x}^T \boldsymbol{y}$
$< \boldsymbol{x}, \boldsymbol{y} >_L$	It denotes $\boldsymbol{x}^T \boldsymbol{L} \boldsymbol{y}$
$\|\boldsymbol{x}\|_L^2$	It denotes $\boldsymbol{x}^T \boldsymbol{L} \boldsymbol{x}$
$\boldsymbol{X} \succeq \boldsymbol{Y}$	$\boldsymbol{X} - \boldsymbol{Y}$ is semi-positive definite.
$\boldsymbol{X} = \text{diag}(x_1, ..., x_n)$	A square diagonal matrix with the elements $x_1, ..., x_n$ on the main diagonal.
$\sigma_{\min}(\cdot)$	It denotes the smallest eigenvalue.

let r_{ij} and x_{ij} denote its resistance and reactance, P_{ij} and Q_{ij} denote the real and reactive power flows from bus i to j, respectively. Also, let $\mathcal{N}_j$ denote the set of all buses located strictly after bus j along the radial network. The branch flow model [28] to model this radial distribution network flow is given for $\forall(i, j) \in \mathcal{L}$ as follows:

$$P_{ij} - \sum_{k \in \mathcal{N}_j} P_{jk} = -p_j + r_{ij} \frac{P_{ij}^2 + Q_{ij}^2}{V_i^2} \quad (1a)$$

$$Q_{ij} - \sum_{k \in \mathcal{N}_j} Q_{jk} = -q_j + x_{ij} \frac{P_{ij}^2 + Q_{ij}^2}{V_i^2} \quad (1b)$$

$$V_i^2 - V_j^2 = 2(r_{ij} P_{ij} + x_{ij} Q_{ij})$$
$$- (r_{ij}^2 + x_{ij}^2) \frac{P_{ij}^2 + Q_{ij}^2}{V_i^2} \quad (1c)$$

And we further define the column vectors $\boldsymbol{V} = [V_i]_{i \in \mathcal{N}}$, $\boldsymbol{p} = [p_i]_{i \in \mathcal{N}}$, $\boldsymbol{q} = [q_i]_{i \in \mathcal{N}}$, $\boldsymbol{P} = [P_{b^p(j)j}]_{(b^p(j), j) \in \mathcal{L}}$, $\boldsymbol{Q} = [Q_{b^p(j)j}]_{(b^p(j), j) \in \mathcal{L}}$.[1] Before rigorously formulating the VVC problem, we separate $\boldsymbol{q} = \boldsymbol{q}^g - \boldsymbol{q}^c$ into two parts, i.e., $\boldsymbol{q}^g$ and $\boldsymbol{q}^c$, where $\boldsymbol{q}^g$, $\boldsymbol{q}^c$ denote the reactive power contributed by DERs and any other load reactive power consumption, respectively. The nonlinear power flow relationships existing in (1) are compactly expressed as follows:

$$\boldsymbol{V} = h(\boldsymbol{q}^g, \boldsymbol{d}) \quad (2)$$

where $\boldsymbol{d} = \{\boldsymbol{q}^c, \boldsymbol{p}\}$. The VVC problem, based on the nonlinear power flow, aims to mitigate the voltage deviations by controlling VAr outputs of DERs. It is represented as follows:

$$\min_{\boldsymbol{q}^g} m(\boldsymbol{q}^g) = \frac{1}{2} \|h(\boldsymbol{q}^g, \boldsymbol{d}) - \boldsymbol{V}_r\|_{\boldsymbol{\Phi}}^2 \quad (3a)$$

$$\text{s.t. } \underline{\boldsymbol{q}}^g \leq \boldsymbol{q}^g \leq \overline{\boldsymbol{q}}^g \quad (3b)$$

where $\boldsymbol{V}_r \in \mathbb{R}^m$ is the reference of voltage magnitude, $\boldsymbol{\Phi}$ is a symmetric positive-definite matrix, (3b) denotes VAr limits for DERs. However, this VVC problem is non-convex due to the nonlinear power flow $h(\boldsymbol{q}^g, \boldsymbol{d})$, which is challenging to solve.

To facilitate the algorithm design and theoretical analysis, the linearized distribution power flow is adopted [2]:

$$P_{ij} - \sum_{k \in \mathcal{N}_j} P_{jk} = -p_j, Q_{ij} - \sum_{k \in \mathcal{N}_j} Q_{jk} = -q_j \quad (4a)$$

---

[1] The real and reactive power flows over line segments ℓ_j are sorted in accordance with the ordering of these line segments from small to large j. The bus voltage magnitudes and real/reactive power injections are sorted in accordance with the ordering of these buses from small to large j.

[2] It is based on two assumptions: (1) The loss is negligible compared to the line flow; (2) With respect to the relatively flat voltage profile, i.e., $V_i \approx 1$, for $\forall i \in \mathcal{N}$, we have $V_i^2 - V_j^2 = 2(V_i - V_j)$. The approximation error introduced by the two assumptions is relatively small [23]

$$V_i - V_j = r_{ij}P_{ij} + x_{ij}Q_{ij} \tag{4b}$$

Consider the standard matrix representation $\bar{M} = [\boldsymbol{m}_0, \boldsymbol{M}^T]^T \in \mathbb{R}^{(N+1) \times N}$ for the incidence matrix of a radial distribution network.[3] Based on $\bar{M}$, this linearized distribution power flow can be compactly denoted by:

$$\boldsymbol{V} = \boldsymbol{M}^{-T}\boldsymbol{R}\boldsymbol{M}^{-1}\boldsymbol{p} + \boldsymbol{M}^{-T}\boldsymbol{X}\boldsymbol{M}^{-1}\boldsymbol{q} - V_0\boldsymbol{M}^{-T}\boldsymbol{m}_0 \tag{5}$$

where $\boldsymbol{R}$ and $\boldsymbol{X}$ are $N \times N$ diagonal matrices with j-th diagonal entries being the resistance and reactance of ℓ_j, respectively. Let $\boldsymbol{A} = \boldsymbol{M}^{-T}\boldsymbol{X}\boldsymbol{M}^{-1}$ and $\boldsymbol{V}^{par}(\boldsymbol{d}) = \boldsymbol{M}^{-T}\boldsymbol{R}\boldsymbol{M}^{-1}\boldsymbol{p} - \boldsymbol{A}\boldsymbol{q}^c - V_0\boldsymbol{M}^{-T}\boldsymbol{m}_0$, (5) can be denoted by:

$$\boldsymbol{V} = h_l(\boldsymbol{q}^g, \boldsymbol{d}) = \boldsymbol{A}\boldsymbol{q}^g + \boldsymbol{V}^{par}(\boldsymbol{d}) \tag{6}$$

We further define $f(\boldsymbol{q}^g)$ as follows:

$$\begin{aligned} f(\boldsymbol{q}^g) &= \frac{1}{2}||h_l(\boldsymbol{q}^g, \boldsymbol{d}) - \boldsymbol{V}_r||_\Phi^2 \\ &= \frac{1}{2}||\boldsymbol{A}\boldsymbol{q}^g + \boldsymbol{V}^{par}(\boldsymbol{d}) - \boldsymbol{V}_r||_\Phi^2 \end{aligned} \tag{7}$$

And let $g(\boldsymbol{q}^g)$ denote the indicator function of the box constraints $\underline{\boldsymbol{q}}^g \le \boldsymbol{q}^g \le \overline{\boldsymbol{q}}^g$. This VVC problem[4], based on the linearized distribution power flow (6), is represented as follows:

$$\min_{\boldsymbol{q}^g} F(\boldsymbol{q}^g) = f(\boldsymbol{q}^g) + g(\boldsymbol{q}^g) \tag{8}$$

Note that $\boldsymbol{M}$ is a symmetric positive-definite matrix [23], it follows that $\boldsymbol{A} = \boldsymbol{M}^{-T}\boldsymbol{X}\boldsymbol{M}^{-1}$ is a symmetric positive-definite matrix, indicating $f(\boldsymbol{q}^g)$ is convex. The VVC problem (8) turns out to be a box-constrained convex program.

Remark 1: The linearized distribution power flow (5) is adopted to facilitate the algorithm design and theoretical analysis. Note that our proposed voltage control can also be applied to the nonlinear distribution power flow model (1). In our numerical case studies, we test the performance of our proposed voltage control on the nonlinear power flow model.

III. Voltage Control Using Generalized Fast Gradient Method

In this section, we propose a GFGM-based VVC strategy to solve the VVC problem. The GFGM-based VVC strategy is the basis for designing automatic local self-adaptive voltage control. *The GFGM-based VVC strategy can be equivalently converted into automatic local self-adaptive voltage control by designing proper parameters, which will be discussed in detail in Section IV.* The stability, convergence and optimality properties of the GFGM-based VVC strategy also apply to the proposed automatic local self-adaptive voltage control.

[3] A simple numerical example illustrating the construction of $\bar{M}$ for a radial distribution network is given in [29, Appendix C].

[4] For this VVC problem, we do not consider the hard voltage constraint, but instead treat the voltage constraint as a soft penalty in the objective to facilitate the algorithm design, like [13], [23]

Algorithm 1 GFGM-Based VVC

Initialization: Set the iteration time $k = 0$, and $\gamma(1) = 1$, $\boldsymbol{q}^g(0) = \boldsymbol{y}(1) = \boldsymbol{0}$.
For $k \ge 1$: Alternately update variables by the following steps (S1)-(S3) until convergence:
S1: Update $\boldsymbol{q}^g(k)$:

$$\boldsymbol{q}^g(k) = p_{\boldsymbol{L}}(\boldsymbol{y}(k)) = \arg\min_{\boldsymbol{q}^g} Q_{\boldsymbol{L}}(\boldsymbol{q}^g, y)$$

S2: Update $\gamma(k+1)$:

$$\gamma(k+1) = \frac{1 + \sqrt{1 + 4\gamma(k)^2}}{2}$$

S3: Update $\boldsymbol{y}(k+1)$:

$$\boldsymbol{y}(k+1) = \boldsymbol{q}^g(k) + \left[\frac{\gamma(k) - 1}{\gamma(k+1)}\right]\left[\boldsymbol{q}^g(k) - \boldsymbol{q}^g(k-1)\right]$$

A. GFGM-Based Volt/Var Control

For a box-constrained convex program, it is suitable to solve it by means of GP methods, but the convergence rate of GP is relatively slow [24], [25], which is typically characterized by $O(1/k)$ (k is the iteration number). To improve the convergence performance, we apply the generalized fast gradient method [26], [27] to solve this VVC problem (8) with a global rate of convergence, which is proven to be significantly better compared to traditional GP methods.

Before applying GFGM to solve this VVC problem (8), we first introduce the concept of the approximation model, which is defined as follows:

Definition: Approximation model of $F(\boldsymbol{q}^g)$. Given a symmetric positive-definite matrix $\boldsymbol{L}$, we say $Q_{\boldsymbol{L}}(\boldsymbol{q}^g, \boldsymbol{y})$ is the quadratic approximation model of $F(\boldsymbol{q}^g)$ at a given point $\boldsymbol{y}$ if $Q_{\boldsymbol{L}}(\boldsymbol{q}^g, \boldsymbol{y})$ satisfies:

$$\begin{aligned} F(\boldsymbol{q}^g) &\le Q_{\boldsymbol{L}}(\boldsymbol{q}^g, \boldsymbol{y}) \\ &= f(\boldsymbol{y}) + <\nabla f(\boldsymbol{y}), \boldsymbol{q}^g - \boldsymbol{y}> + \frac{1}{2}||\boldsymbol{q}^g - \boldsymbol{y}||_{\boldsymbol{L}}^2 + g(\boldsymbol{q}^g) \end{aligned} \tag{9}$$

where

$$<\nabla f(\boldsymbol{y}), \boldsymbol{q}^g - \boldsymbol{y}> = [\nabla f(\boldsymbol{y})]^T(\boldsymbol{q}^g - \boldsymbol{y}), \text{ and}$$
$$||\boldsymbol{q}^g - \boldsymbol{y}||_{\boldsymbol{L}}^2 = (\boldsymbol{q}^g - \boldsymbol{y})^T\boldsymbol{L}(\boldsymbol{q}^g - \boldsymbol{y})$$

And let $p_{\boldsymbol{L}}(\boldsymbol{y})$ be:

$$p_{\boldsymbol{L}}(\boldsymbol{y}) = \arg\min_{\boldsymbol{q}^g} Q_{\boldsymbol{L}}(\boldsymbol{q}^g, y) \tag{10}$$

Based on the definitions of $Q_{\boldsymbol{L}}(\boldsymbol{q}^g, \boldsymbol{y})$ and $p_{\boldsymbol{L}}(\boldsymbol{y})$, the specific steps of applying GFGM to solve this VVC problem (8) are given in Algorithm 1: GFGM-Based VVC.

B. Stability, Convergence and Optimality Analyses

The stability, convergence and optimality properties of Algorithm 1: GFGM-Based VVC, are established on Propositions 1-4.

Proposition 1: Assume that $f(\boldsymbol{q}^g) : \mathbb{R}^N \to \mathbb{R}$ is convex and continuously differentiable and $\boldsymbol{L}$ is a symmetric positive-definite matrix. The condition that:

$$f(\boldsymbol{q}^g) \le f(\boldsymbol{y}) + <\nabla f(\boldsymbol{y}), \boldsymbol{q}^g - \boldsymbol{y}> + \frac{1}{2}||\boldsymbol{q}^g - \boldsymbol{y}||_{\boldsymbol{L}}^2 \tag{11}$$

holds for all $\boldsymbol{q}^g, \boldsymbol{y} \in \mathbb{R}^N$ is equivalent to that:

$$< \nabla f(\boldsymbol{q}^g) - \nabla f(\boldsymbol{y}), \boldsymbol{q}^g - \boldsymbol{y} > \leq ||\boldsymbol{q}^g - \boldsymbol{y}||_L^2 \quad (12)$$

holds for all $\boldsymbol{q}^g, \boldsymbol{y} \in \mathbb{R}^N$.

Proof of Proposition 1: See Appendix A.

Proposition 2: Suppose $F(\boldsymbol{q}^g) = f(\boldsymbol{q}^g) + g(\boldsymbol{q}^g)$ satisfies the following conditions:

- **[P2.A]** $g(\boldsymbol{q}^g)$ is a convex function which may not be differentiable.
- **[P2.B]** $f(\boldsymbol{q}^g)$ is convex and continuously differentiable.
- **[P2.C]** $Q_L(\boldsymbol{q}^g, y)$ is the quadratic approximation model of $F(\boldsymbol{q}^g)$

Then the sequence $\{\boldsymbol{q}^g(k)\}$, generated by Algorithm 1: GFGM-Based VVC, satisfies:

$$F(\boldsymbol{q}^g(k)) - F(\boldsymbol{q}^{g*}) \leq \frac{2||\boldsymbol{q}^g(0) - \boldsymbol{q}^{g*}||_L^2}{(k+1)^2}, \forall k \geq 1 \quad (13)$$

where $\boldsymbol{q}^{g*}$ is the optimal solution of (8),

Proof of Proposition 2: Proposition 2 can be easily proved by replacing $L < \cdot, \cdot >$ and $L|| \cdot ||^2$ in the proofs in [26] with $< \cdot, \cdot >_L$ and $|| \cdot ||_L^2$. Q.E.D.

With respect to Proposition 2, as conditions [P2.A]-[P2.C] hold, it shows Algorithm 1 GFGM-Based VVC can achieve a convergence rate no worse than $O(1/(k+1)^2)$, it exhibits a fast convergence rate compared to GP methods with the convergence rate $O(1/k)$. Note that [P2.A] holds since the indicator function of the convex set $\underline{\boldsymbol{q}}^g \leq \boldsymbol{q}^g \leq \overline{\boldsymbol{q}}^g$ is a convex function. Additionally, $\nabla^2 f(\boldsymbol{q}^g) = \boldsymbol{A}\Phi\boldsymbol{A}$ is positive definite as Φ and $\boldsymbol{A}$ are both symmetric positive definite matrices, indicating [P2.B] holds. ***One remaining challenge is [P2.C].*** Note that from Proposition 1, we know that as long as $\boldsymbol{L}$ satisfies (12), then [P2.C] will hold. Thus, to satisfy [P2.C], the symmetric positive-definite matrix $\boldsymbol{L}$ is required to satisfy (12). From (7), we have:

$$\nabla f(\boldsymbol{q}^g) = \boldsymbol{A}\Phi[\boldsymbol{A}\boldsymbol{q}^g + \boldsymbol{c}(\boldsymbol{d}) - \boldsymbol{V}_r] \quad (14)$$

It follows that:

$$< \nabla f(\boldsymbol{q}^g) - \nabla f(\boldsymbol{y}), \boldsymbol{q}^g - \boldsymbol{y} > = ||\boldsymbol{q}^g - \boldsymbol{y}||_{\boldsymbol{A}\Phi\boldsymbol{A}}^2 \quad (15)$$

From (15), it follows that (12) is satisfied if the condition (16) holds:

$$\boldsymbol{L} \succeq \boldsymbol{A}\Phi\boldsymbol{A} \quad (16)$$

i.e., $\boldsymbol{L} - \boldsymbol{A}\Phi\boldsymbol{A}$ is semi-positive definite.

Proposition 3: Suppose $F(\boldsymbol{q}^g) = f(\boldsymbol{q}^g) + g(\boldsymbol{q}^g)$ satisfies the following conditions:

- **[P3.A]** [P2.A]-[P2.C] hold.
- **[P3.B]** $g(\boldsymbol{q}^g)$ is an indicator function, and for $\forall \boldsymbol{q}^g, \boldsymbol{y} \in \mathbb{R}^N$, there exists a positive definite matrix $\boldsymbol{H}$ satisfying:

$$< \nabla f(\boldsymbol{q}^g) - \nabla f(\boldsymbol{y}), \boldsymbol{q}^g - \boldsymbol{y} > \geq ||\boldsymbol{q}^g - \boldsymbol{y}||_{\boldsymbol{H}}^2 \quad (17)$$

Then the sequence $\{\boldsymbol{q}^g(k)\}$, generated by Algorithm 1: GFGM-Based VVC, satisfies:

$$||\boldsymbol{q}^g(k) - \boldsymbol{q}^{g*}|| \leq \frac{2||\boldsymbol{q}^g(0) - \boldsymbol{q}^{g*}||_L}{(k+1)\sqrt{\sigma_{\min}(\boldsymbol{H})}} \quad (18)$$

where $\sigma_{\min}(\cdot)$ denotes the smallest eigenvalue.

Proof of Proposition 3: See Appendix B.

With respect to Proposition 3, it shows $\boldsymbol{q}^g(k)$ will finally converge to the optimal solution $\boldsymbol{q}^{g*}$, indicating the system is stable when [P3.A] and [P3.B] hold. The condition [P3.A], i.e., [P2.A]-[P2.C], has been discussed in the previous analysis regarding Proposition 2. With respect to [P3.B], it follows from (7) that:

$$< \nabla f(\boldsymbol{q}^g) - \nabla f(\boldsymbol{y}), \boldsymbol{q}^g - \boldsymbol{y} > = ||\boldsymbol{q}^g - \boldsymbol{y}||_{\boldsymbol{A}\Phi\boldsymbol{A}}^2 \quad (19)$$

It is clear that [P3.B] always holds as we set $\boldsymbol{H} = \boldsymbol{A}\Phi\boldsymbol{A}$.

In short, with respect to the VVC problem (8), we can conclude that as long as $\boldsymbol{L} \succeq \boldsymbol{A}\Phi\boldsymbol{A}$ holds, Propositions 2 and 3 will hold.

Note that the linearized distribution power flow model is leveraged to convexify the optimal power flow problem and facilitate the algorithm design and theoretical analysis. *In Proposition 4, we further analyze the overall performance of Algorithm 1: GFGM-Based VVC on the actual nonlinear power flow.*

Proposition 4: Let $\hat{\boldsymbol{q}}^{g*}$, $m(\hat{\boldsymbol{q}}^{g*})$ be the optimal solution and value of problem (3), and $\boldsymbol{q}^{g*}$, $f(\boldsymbol{q}^{g*})$ be the optimal solution and value of problem (8). Assume the following conditions hold:

- **[P4.A]** The error between the linearized power flow model and the exact nonlinear power flow model is bounded. That is, there exists a $\delta < \infty$ satisfying

$$||h(\boldsymbol{q}^g, \boldsymbol{d}) - h_l(\boldsymbol{q}^g, \boldsymbol{d})||_2 \leq \delta, \text{where } \underline{\boldsymbol{q}}^g \leq \boldsymbol{q}^g \leq \overline{\boldsymbol{q}}^g$$

- **[P4.B]** The error between the optimal objective values of problem (3) and problem (8) is bounded. That is, there exists a $\tau < \infty$ satisfying

$$\left| m(\hat{\boldsymbol{q}}^{g*}) - f(\boldsymbol{q}^{g*}) \right| \leq \tau$$

- **[P4.C]** [P2.A]-[P2.C] hold.

Then, it follows that:

$$m(\boldsymbol{q}^g(k)) - m(\hat{\boldsymbol{q}}^{g*}) \leq \frac{1}{2}||\boldsymbol{E}||_2^2\delta^2 + \frac{2||\boldsymbol{q}^g(0) - \boldsymbol{q}^{g*}||_L^2}{(k+1)^2} + \tau \quad (20)$$

where $\boldsymbol{E}$, satisfying $\boldsymbol{E}^T\boldsymbol{E} = \Phi$, is an upper triangular matrix with real and positive diagonal entries.

Proof of Proposition 4: See Appendix C.

In Proposition 4, $m(\boldsymbol{q}^g(k))$ can be regarded as the objective value in the actual nonlinear power flow system after implementing $\boldsymbol{q}^g(k)$, which is determined based on the linearized power flow. Proposition 4 shows that the gap between $m(\boldsymbol{q}^g(k))$ and $m(\hat{\boldsymbol{q}}^{g*})$ is always bounded by three terms: (i) The error τ between the optimal values of problem (3) considering the linearized power flow constraints, and problem (8) considering the nonlinear power flow constraints; (ii) $\frac{1}{2}||E||_2^2\delta^2$ is in proportion to δ^2; (iii) $\frac{2||\boldsymbol{q}^g(0)-\boldsymbol{q}^{g*}||_L^2}{(k+1)^2}$ decreases as k increases.

IV. AUTOMATIC SELF-ADAPTIVE LOCAL VOLTAGE CONTROL DESIGN

A. Overview

In this section, we mainly focus on the transition from Algorithm 1: GFGM-Based VVC to the self-adaptive local voltage

control design. Note that γ in **S2** of Algorithm 1: GFGM-Based VVC can be simultaneously updated by each bus agent. And **S3** in Algorithm 1: GFGM-Based VVC is naturally decomposable, which can be locally updated by each bus agent i in the way:

$$y_i(k+1) = q_i^g(k) + \left[\frac{\gamma(k)-1}{\gamma(k+1)}\right]\left[q_i^g(k) - q_i^g(k-1)\right], \forall i \in \mathcal{N} \tag{21}$$

However, **S1** in Algorithm 1: GFGM-Based VVC is not naturally decomposable. The key challenge for local voltage control is how to design Φ and $\boldsymbol{L}$ such that **S1** in Algorithm 1: GFGM-Based VVC can also be locally implemented by each bus agent.

B. Selection of Φ and $\boldsymbol{L}$

Regarding the choice of Φ and $\boldsymbol{L}$, there are two main considerations: (i) Φ and $\boldsymbol{L}$ should satisfy (16) to make [P2.C] hold, thus ensuring the stability, convergence and optimality properties of voltage control; (ii) Under the selected Φ and $\boldsymbol{L}$, **S1** in Algorithm 1: GFGM-Based VVC can be locally implemented.

To this end, we first design $\boldsymbol{L}$ as a diagonal positive definite matrix, i.e., $\boldsymbol{L} = \text{diag}(L_1, ..., L_N)$. As shown in Proposition 5, the diagonal positive definite matrix $\boldsymbol{L}$ contributes to the local implementation of $\boldsymbol{q}^g(k) = p_{\boldsymbol{L}}(\boldsymbol{y}(k))$ in **S1** of Algorithm 1: GFGM-Based VVC.

Proposition 5: As $\boldsymbol{L}$ is a diagonal positive definite matrix, $\boldsymbol{q}^g(k) = p_{\boldsymbol{L}}(\boldsymbol{y}(k))$ in **S1** of Algorithm 1: GFGM-Based VVC is equivalent to:

$$q_i^g(k) = \left[y_i(k) - \frac{1}{L_i}\frac{\partial f(\boldsymbol{y}(k))}{\partial y_i(k)}\right]_{\underline{q}_i(k)}^{\overline{q}_i(k)}, \forall i \in \mathcal{N} \tag{22}$$

which can be expressed in a compact form:

$$\boldsymbol{q}^g(k) = [\boldsymbol{y}(k) - \boldsymbol{L}^{-1}\nabla f(\boldsymbol{y}(k))]_{\underline{\boldsymbol{q}}^g}^{\overline{\boldsymbol{q}}^g} \tag{23}$$

Proof of Proposition 5: See Appendix D.

With respect to (22), the remaining challenge for the local implementation of $\boldsymbol{q}^g(k) = p_{\boldsymbol{L}}(\boldsymbol{y}(k))$ is locally calculating $\frac{\partial f(\boldsymbol{y}(k))}{\partial y_i(k)}$ when $\boldsymbol{L}$ is a diagonal positive definite matrix.

Next, we further discuss how to choose $\boldsymbol{L}$ and Φ to resolve the dilemma: the local implementation of calculating $\frac{\partial f(\boldsymbol{y}(k))}{\partial y_i(k)}$. From (15), it follows that:

$$\nabla f(\boldsymbol{y}(k)) = \boldsymbol{A}\Phi[\boldsymbol{A}\boldsymbol{y}(k) + \boldsymbol{c} - \boldsymbol{V}_r] \tag{24}$$

It is obtained from Algorithm 1: GFGM-Based VVC that:

$$\boldsymbol{y}(k) = \begin{cases} \boldsymbol{q}^g(0) = \boldsymbol{0}, k = 1 \\ \boldsymbol{q}^g(k-1) + \\ \left[\frac{\gamma(k-1)-1}{\gamma(k)}\right]\left[\boldsymbol{q}^g(k-1) - \boldsymbol{q}^g(k-2)\right], k \geq 2 \end{cases} \tag{25}$$

Substituting (25) into $\boldsymbol{A}\boldsymbol{y}(k) + \boldsymbol{c} - \boldsymbol{V}_r$:

$$\boldsymbol{A}\boldsymbol{y}(1) + \boldsymbol{c} - \boldsymbol{V}_r = \boldsymbol{A}\boldsymbol{q}^g(0) + \boldsymbol{c} - \boldsymbol{V}_r = \boldsymbol{V}(0) - \boldsymbol{V}_r \tag{26a}$$

$$\boldsymbol{A}\boldsymbol{y}(k) + \boldsymbol{c} - \boldsymbol{V}_r = \left[1 + \frac{\gamma(k-1)-1}{\gamma(k)}\right]\left[\boldsymbol{A}\boldsymbol{q}^g(k-1) + \boldsymbol{c} - \boldsymbol{V}_r\right]$$
$$- \frac{\gamma(k-1)-1}{\gamma(k)}\left[\boldsymbol{A}\boldsymbol{q}^g(k-2) + \boldsymbol{c} - \boldsymbol{V}_r\right]$$
$$= \left[1 + \frac{\gamma(k-1)-1}{\gamma(k)}\right]\left[\boldsymbol{V}(k-1) - \boldsymbol{V}_r\right]$$

$$- \frac{\gamma(k-1)-1}{\gamma(k)}[\boldsymbol{V}(k-2) - \boldsymbol{V}_r], k \geq 2 \tag{26b}$$

As we set $\Phi = \boldsymbol{A}^{-1}$, (24) can be expressed as follows:

$$\nabla f(\boldsymbol{y}(1)) = \boldsymbol{V}(0) - \boldsymbol{V}_r \tag{27a}$$

$$\nabla f(\boldsymbol{y}(k)) = \left[1 + \frac{\gamma(k-1)-1}{\gamma(k)}\right][\boldsymbol{V}(k-1) - \boldsymbol{V}_r]$$

$$- \frac{\gamma(k-1)-1}{\gamma(k)}[\boldsymbol{V}(k-2) - \boldsymbol{V}_r], k \geq 2 \tag{27b}$$

Thus, for $\forall i \in \mathcal{N}$, $\frac{\partial f(\boldsymbol{y}(k))}{\partial y_i(k)}$ can be calculated locally by:

$$\frac{\partial f(\boldsymbol{y}(1))}{\partial y_i(1)} = V_i(0) - V_r \tag{28a}$$

$$\frac{\partial f(\boldsymbol{y}(k))}{\partial y_i(k)} = \left[1 + \frac{\gamma(k-1)-1}{\gamma(k)}\right][V_i(k-1) - V_r]$$

$$- \frac{\gamma(k-1)-1}{\gamma(k)}[V_i(k-2) - V_r], k \geq 2 \tag{28b}$$

It is clear that $\frac{\partial f(\boldsymbol{y}(k))}{\partial y_i(k)}$ can be locally updated by each bus i in (28).

From the above analysis, we can conclude that **S1** in Algorithm 1: GFGM-Based VVC can be locally implemented with a diagonal positive definite matrix $\boldsymbol{L}$ and $\Phi = \boldsymbol{A}^{-1}$. Moreover, with respect to the choice of $\boldsymbol{L}$, Φ and $\boldsymbol{L}$ should satisfy (16), thus we have:

$$\boldsymbol{L} \succeq \boldsymbol{A}\boldsymbol{A}^{-1}\boldsymbol{A} = \boldsymbol{A} \tag{29}$$

$\boldsymbol{L} = \boldsymbol{A}$ provides the tightest bound $Q_{\boldsymbol{L}}(\boldsymbol{q}^g, \boldsymbol{y})$ for $F(\boldsymbol{q}^g)$, the best convergence performance of GFGM can be expected. However, such a selection cannot facilitate the local implementation of **S1** in Algorithm 1: GFGM-Based VVC. Instead $\boldsymbol{L}$ should be a diagonal positive definite matrix satisfying $\boldsymbol{L} \succeq \boldsymbol{A}$. Consequently, we utilize the following convex semi-definite programming problem to determine $\boldsymbol{L}$:

$$\min_{\boldsymbol{L}} \text{tr}\boldsymbol{L} = \sum_{i=1}^{N} L_i \tag{30a}$$

$$\text{s.t. } \boldsymbol{L} \succeq \boldsymbol{A}, \boldsymbol{L} = \text{diag}(L_1, ..., L_N) \tag{30b}$$

Remark 2: In a nutshell, we select $\Phi = \boldsymbol{A}^{-1}$ and $\boldsymbol{L}$, determined by (30). Such a choice not only satisfies (16) to hold [P2.C], but also facilitates the local implementation of Algorithm 1 :GFGM-Based VVC.

C. Reinterpretation of GFGM: Modified Droop Control

For ease of expression and analysis, we introduce $\mu(k)$ and $\boldsymbol{b}(k)$ as follows:

$$\mu(k) = \begin{cases} 0, k = 1 \\ \frac{\gamma(k-1)-1}{\gamma(k)}, k \geq 2 \end{cases} \tag{31a}$$

$$\boldsymbol{b}(k) = \begin{cases} \boldsymbol{q}^g(0), k = 1 \\ [1 + \mu(k)]\boldsymbol{q}^g(k-1) - \mu(k)\boldsymbol{q}^g(k-2) \\ + \mu(k)\boldsymbol{L}^{-1}[\boldsymbol{V}(k-2) - \boldsymbol{V}_r], k \geq 2 \end{cases} \tag{31b}$$

Substituting (25) and (27) into (23), we have:

$$\boldsymbol{q}^g(1) = \left[-\boldsymbol{L}^{-1}[\boldsymbol{V}(0) - \boldsymbol{V}_r] + \boldsymbol{q}^g(0)\right]_{\underline{\boldsymbol{q}}^g}^{\overline{\boldsymbol{q}}^g}$$

Algorithm 2 Automatic Self-Adaptive Local Voltage Control (ASALVC): Offline Implementation

---

Initialization: Set the iteration time $k = 0$. Each bus i sets $\gamma(1) = 1$, $q_i^g(0) = y_i(1) = 0$,

For $k \geq 1$: Each bus i alternately update variables by the following steps until convergence:

- Update $\mu(k)$, $a_i(k)$, $b_i(k)$ by (31a), (34a), (34b), respectively.

- Update $q_i^g(k)$ by (33), based on $V_i(k-1)$.

- Update $\gamma(k+1)$:

$$\gamma(k+1) = \frac{1 + \sqrt{1 + 4\gamma(k)^2}}{2}$$

Algorithm 3 Automatic Self-Adaptive Local Voltage Control (ASALVC): Online Implementation

---

For any bus i at time step t:

- Estimate VAr Limits: Locally update $\underline{q}_i^g$ and $\overline{q}_i^g$
- Reset $\gamma(t)$: If $t \bmod T_\gamma = 0$, then set $\gamma(t) = 1$.
- Reset $\mu(t)$: If $t \bmod T_\gamma = 0$, then set $\mu(t) = 0$; otherwise update $\mu(t)$ by $\frac{\gamma(t-1)-1}{\gamma(t)}$.
- Update $a_i(t)$, $b_i(t)$ by (34a), (34b), respectively.
- Update $q_i^g(t)$ by (33), based on the voltage measurement $V_i(t-1)$ at time $t - 1$.
- Update $\gamma(t+1)$:
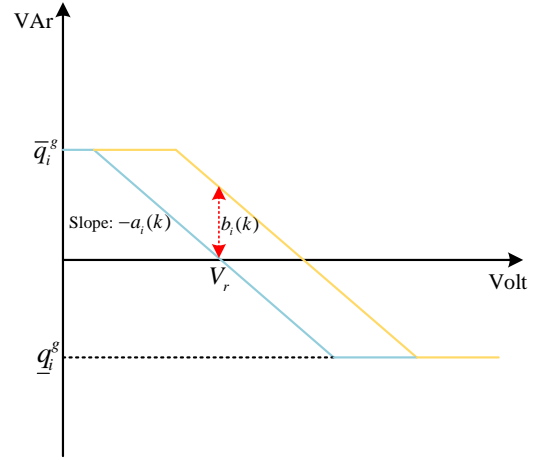
$$\gamma(t+1) = \frac{1 + \sqrt{1 + 4\gamma(t)^2}}{2}$$

$$= \left[-[1 + \mu(1)]\boldsymbol{L}^{-1}[\boldsymbol{V}(0) - \boldsymbol{V}_r] + \boldsymbol{b}(1) \right]_{\underline{\boldsymbol{q}}^g}^{\overline{\boldsymbol{q}}^g} \quad (32a)$$

$$\boldsymbol{q}^g(k) = \left[-[1 + \mu(k)]\boldsymbol{L}^{-1}[\boldsymbol{V}(k-1) - \boldsymbol{V}_r] \right.$$
$$\left. + \boldsymbol{y}(k) + \mu(k)\boldsymbol{L}^{-1}[\boldsymbol{V}(k-2) - \boldsymbol{V}_r] \right]_{\underline{\boldsymbol{q}}^g}^{\overline{\boldsymbol{q}}^g}$$

$$= \left[-[1 + \mu(k)]\boldsymbol{L}^{-1}[\boldsymbol{V}(k-1) - \boldsymbol{V}_r] + \boldsymbol{b}(k) \right]_{\underline{\boldsymbol{q}}^g}^{\overline{\boldsymbol{q}}^g}, k \geq 2 \quad (32b)$$

For $\forall i \in \mathcal{N}$, it follows from (32) that:

$$q_i^g(k) = \left[-a_i(k)[V_i(k-1) - V_r] + b_i(k) \right]_{\underline{q}_i^g}^{\overline{q}_i^g}, k \geq 1 \quad (33)$$

with

$$a_i(k) = \frac{1 + \mu(k)}{L_i}, k \geq 1 \quad (34a)$$

$$b_i(k) = \begin{cases} q_i^g(0), k = 1 \\ [1 + \mu(k)]q_i^g(k-1) - \mu(k)q_i^g(k-2) \\ \quad + \frac{\mu(k)}{L_i}[V_i(k-2) - V_r], k \geq 2 \end{cases} \quad (34b)$$

Note that *both $a_i(k)$ and $b_i(k)$ are updated locally by bus i without the need for communication, only relying on the previous VAr outputs and voltage measurements of bus i.* In this case, *Algorithm 1: GFGM-Based VVC* is equivalent to *Algorithm 2: Automatic Self-Adaptive Local Voltage Control (ASALVC): Offline Implementation.*

Remark 3: Interestingly, this local voltage described in Algorithm 2 can be regarded as *a modified voltage droop control with bus-specific self-adaptive coefficients.* As shown in Fig.1, the modified droop control (the yellow line segments) for bus i is translated from the blue line segments with the slope $-a_i(k)$.

Remark 4: The proposed ASALVC is equivalent to the GFGM-Based VVC with $\Phi = \boldsymbol{A}^{-1}$ and $\boldsymbol{L}$, determined by (30). As we discussed before, $\Phi = \boldsymbol{A}^{-1}$ and $\boldsymbol{L}$, determined by (30), can always satisfy all the conditions in Propositions 1-4, thus Propositions 1-4 always hold for the ASALVC by setting $\Phi = \boldsymbol{A}^{-1}$ and $\boldsymbol{L}$, determined by (30).

D. Online Implementation

To better deal with the time-varying system variations, associated with the time-varying $\boldsymbol{d}$, the online implementation of Algorithm 2 is proposed in this subsection.

Fig. 1. Modified droop control with bus-specific time-varying coefficients

Remark 5: With respect to offline implementation, the decision/control variables are not applied to the physical world until those variables converge [5]. However, with respect to online implementation, the decision/control variables are adjusted in real-time (for each iteration), based on the real-time feedback from operating statuses, to adapt to real-time changes in the environment.

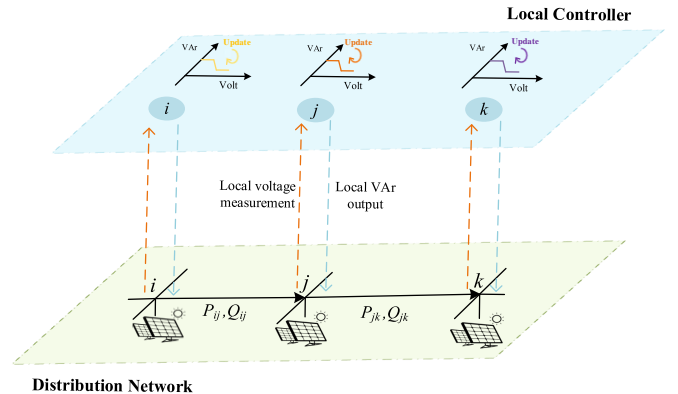The online implementation of ASALVC consists of the following key steps:

Fig. 2. Automatic Self-Adaptive Local Voltage Control Demonstration.

1) Estimate $\underline{q}_i^g$ and $\overline{q}_i^g$: For the online implementation, VAr limits $\underline{q}_i^g$ and $\overline{q}_i^g$ are updated based on the inverter capacities and the instantaneous real power outputs of DERs. This online update of VAr limits ensures to satisfy the inverter capacity limit in a time-varying system, preventing inverters from overloading.

2) Reset γ and μ: With respect to the offline implementation, we usually start with $\gamma = 1$, $\mu = 0$, and then γ is updated in each iteration. For the online implementation, we propose to reset $\gamma = 1$ and $\mu = 0$ every T_γ time steps to ensure the tracking capability.

3) Update a_i, b_i, q_i^g and γ: Update a_i, b_i by (34), q_i^g by (33), γ by $\gamma(t+1) = \frac{1+\sqrt{1+4\gamma(t)^2}}{2}$. With respect to the online implementation, the actual voltage measurement V_i, instead of the one calculated by the linearized distribution power flow, is used to update b_i and q_i^g in (33)-(34).

The details of the online implementation are provided in *Algorithm 3: Automatic Self-Adaptive Local Voltage Control (ASALVC): Online Implementation* and Fig.2. As depicted in Fig.2, each bus agent locally measures its voltage, then updates coefficients, i.e., $a_i(t)$ and $b_i(t)$, of its modified voltage control based on its voltage measurement, and finally determines its local VAr output. As shown in (34), $a_i(t)$ and $b_i(t)$ can be updated online by simple arithmetic based on the previous VAr outputs, $q_i(t-1)$ and $q_i(t-2)$, and the previous voltage measurement $V_i(t-2)$,

Remark 6: Though we design ASALVC and establish its theoretical analysis, based on the linearized distribution power flow, under a fixed condition, the online implementation could asymptotically mitigate the model errors due to the closed-loop nature. More specifically, the online implementation of ASALVC can track changing network conditions as these changes manifest themselves in the network state, i.e., the actual voltage measurement, that is used to compute the control solution, i.e., VAr outputs of DERs.

E. Comparisons with other droop controls

The common existing droop controls can be roughly classified into the following types:

(1) Classical Droop Control [15]-[17] (CDC): As advocated in IEEE 1547-2018 Standard, the CDC adjusts the inverter VAr output based on the instantaneous bus voltage mismatch. The CDC with zero dead band is updated by $q_i(t+1) = \left[-a_i[V_i(t) - V_r] \right]_{\underline{q}_i^g}^{\overline{q}_i^g}$, associated with a constant slope and a constant intercept. But it cannot guarantee optimum and always suffers from stability problems.

(2) Delayed Droop Control [19] (DDC): The DDC can address the instability issues of CDC to a great degree. The VAr output of DDC depends on a weighted combination of the previous voltage and VAr output: $q_i(t+1) = (1-\alpha_i)q_i(t) + \alpha_i\left[-a_i[V_i(t) - V_r] \right]_{\underline{q}_i^g}^{\overline{q}_i^g}$, associated with a constant slope and a time-varying intercept, where $0 < \alpha_i < 1$ is a weighted parameter. However, the work [19] does not provide optimality analyses.

(3) GP-Based Droop Control [22], [23] (GPDC): The GP update is applied to the droop control, thus generating the GPDC. It is updated by $q_i(t+1) = \left[q_i(t) - a_i[V_i(t) - V_r] \right]_{\underline{q}_i^g}^{\overline{q}_i^g}$, associated with a constant slope and a time-varying intercept. Optimality analyses are provided in [22], [23].

(4) Scaled GP-Based Droop Control [23] (SGPDC): The scaled GP update is applied to the droop control to speed up the convergence rate of GPDC, facilitating the development of SGPDC. The inverse of the diagonals of Hessian matrix is always a popular choice to scale gradients. It is updated by $q_i(t+1) = \left[q_i(t) - a_i d_i[V_i(t) - V_r] \right]_{\underline{q}_i^g}^{\overline{q}_i^g}$, associated with a constant slope and a time-varying intercept, where d_i is a scaled parameter. Optimality analyses are provided in [23].

Compared to those droop control methods, the ASALVC is associated with the time-varying slope $-a_i(t)$ and the time-varying intercept $b_i(t)$, significantly increasing the diversity and flexibility of local voltage control. In addition, as discussed in Proposition 2, the convergence rate of ASALVC is characterized by $O(1/k^2)$, it is faster than the GPDC and SGPDC, characterized by $O(1/k)$. The summary of droop control comparisons is provided in Table II.

V. CASE STUDY

A. Overview

In this section, numerical simulations are performed in the modified single-phase IEEE 123-bus test system to validate the effectiveness and superiority of the proposed ASALVC. As shown in Fig.3, PV generators are distributed across the radial distribution network.
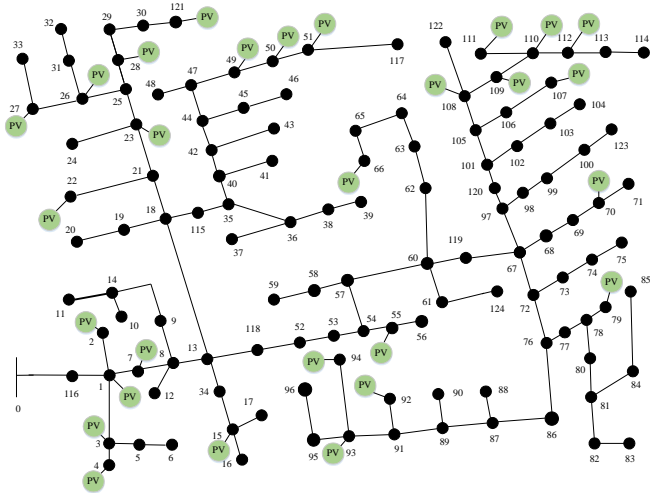

Fig. 3. Modified single-phase IEEE 123-bus test system.

In the numerical simulations, the base voltage for the network is 4.16 kV and the base power is 100 kVA. We set the reference of voltage magnitude as $\boldsymbol{V}_r = \mathbf{1}_N$, a $N \times 1$ column vector of ones. Though the algorithm design of this paper is built on the linearized power flow model (4), we simulate the ASALVC with the nonlinear AC power flow model (1) using MATPOWER [32]. Note that the actual bus voltage magnitude obtained from MATPOWER, instead of the one obtained from the linearized power flow model, is used as the voltage measurement to update the VAr outputs of DERs.

TABLE II
DROOP CONTROL COMPARISONS

Control Type	Update	Description	Optimality
CDC [15]-[17]	$q_i(t+1) = \big[- a_i[V_i(t) - V_r] \big]_{\underline{q}_i^g}^{\overline{q}_i^g}$	Constant slope, constant intercept	w/o analyses
DDC [19]	$q_i(t+1) = (1 - \alpha_i)q_i(t) + \alpha_i \big[- a_i[V_i(t) - V_r] \big]_{\underline{q}_i^g}^{\overline{q}_i^g}$	Constant slope, time-varying intercept	w/o analyses
GPDC[22], [23]	$q_i(t+1) = \big[q_i(t) - a_i[V_i(t) - V_r] \big]_{\underline{q}_i^g}^{\overline{q}_i^g}$	Constant slope, time-varying intercept	w/ analyses
SGPDC[23]	$q_i(t+1) = \big[q_i(t) - a_i d_i[V_i(t) - V_r] \big]_{\underline{q}_i^g}^{\overline{q}_i^g}$	Constant slope, time-varying intercept	w/ analyses
ASALVC	$q_i(t+1) = \big[- a_i(t)[V_i(t) - V_r] + b_i(t) \big]_{\underline{q}_i^g}^{\overline{q}_i^g}$	Time-varying slope, time-varying intercept	w/ analyses

B. Static Scenario

In the static scenario, each bus has a constant load $1 + j0.5$ kVA and each PV inverter can supply or absorb at most 10 kVAr. Different droop controls are considered for comparison, including the CDC, DDC, GPDC, SGPDC, ASALVC. In addition, the centralized optimization is applied to directly solve this VVC problem (8) through the CPLEX solver [33]. For the CDC and GPDC, we set $a_i = 1$. For the DDC, we set $a_i = 1$ and $\alpha_i = 0.1$. For the SGPDC, we set $a_i = 0.01$, $d_i = [\boldsymbol{A}\Phi\boldsymbol{A}]_{ii}^{-1}$, where $[\boldsymbol{A}\Phi\boldsymbol{A}]_{ii}$ is i-th row and i-th column element of $\boldsymbol{A}\Phi\boldsymbol{A}$, where the inverse of the diagonals of Hessian matrix is applied to scale gradients. With respect to the offline implementation of ASALVC in the static scenario, there is no need to manually set droop parameters as those parameters are automatically determined and adjusted by (34).
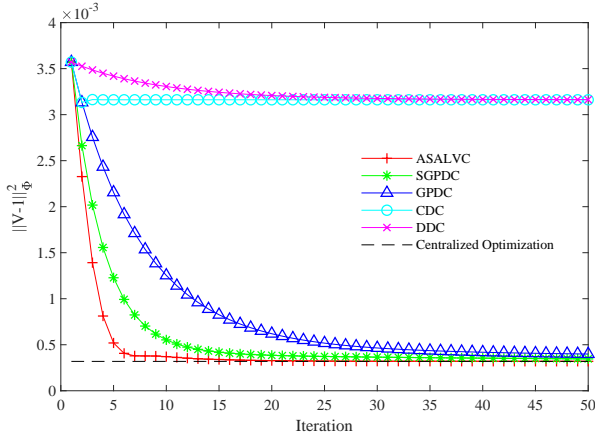

Fig. 4. Voltage mismatch error versus iteration for various VAr controls under the static scenario.

As depicted in Fig.4, the voltage mismatch error of CDC and DDC is around 3×10^{-3}. In contrast, the ASALVC, SG-PDC, GPDC converge to voltage mismatch errors which are far less than the CDC and DDC. The convergence outcomes of ALALVC, SGPDC, and GPDC closely track the centralized optimization outcome, but the convergence outcomes of CDC and DDC do not. As shown in Table II, the design of CDC and DDC does not take into account the optimality property, thus the CDC and DDC do not show a good performance in
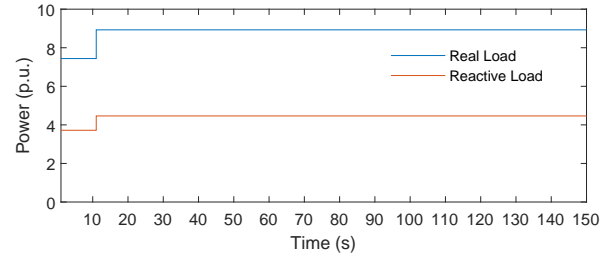

Fig. 5. Aggregate load in the dynamic scenario with a sudden load change.

terms of optimality. Besides, the ASALVC exhibits the best convergence performance compared to other controls, reaching convergence after 6 iterations, which is consistent with our previous theoretical analysis.

C. Dynamic Scenario

In the dynamic scenario, the time-varying system variations are considered. In this scenario, the capacities of PV inverters are set as 50 kVA, and VAr limits $\underline{q}^g, \overline{q}^g$ are updated online based on the given inverter capacities and the instantaneous real power of PV generators. With respect to the online implementation of ASALVC in the dynamic scenario, we set $T_r = 6s$, and the VAr outputs of DERs are updated every second.

First, we consider a sudden load change in the modified IEEE 123-bus test system. As shown in Fig.5, suppose at $t = 10s$, the aggregate load suddenly increases. Taking the voltage at bus 56 as an example, we test the responses from different methods to this sudden load change. For those controls, the parameter settings follow from the static scenario and the VAr outputs of DERs are also updated every second. As shown in Fig.6(a), the system is back to stable operations after some adjustments through the CDC and DDC as there is a sudden load change. However, the stable operating statuses, determined by the CDC and DDC, before and after this sudden load change are both far away from the optimal operating statuses, determined by the centralized optimization, before and after this sudden load change, where the optimal operating statuses are depicted as the black dotted line in Fig.6(b). This is due to the fact the CDC and DDC can only guarantee
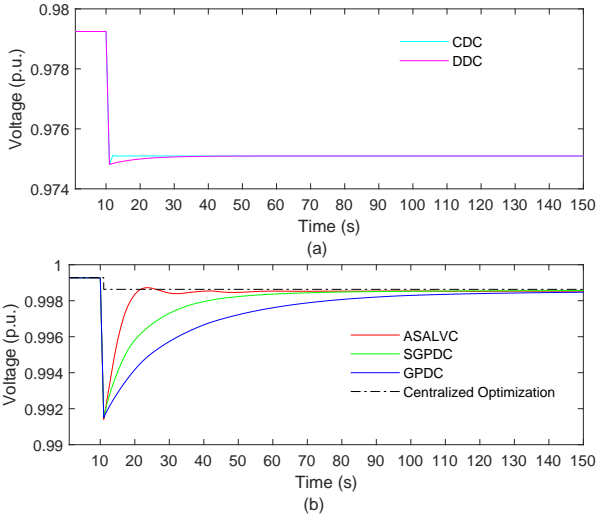
Fig. 6. The voltage at bus 56 under the dynamic scenario with a sudden load change: (a) for the CDC and DDC; (b) for the GPDC, SGPDC, ASALVC, and centralized optimization.

the stability under some conditions but not optimality. On the contrary, as depicted in Fig.6(b), the stable operating statuses, determined by the ASALVC, SGPDC, and GPDC, before and after this sudden load change are the same as the optimal operating statuses, determined by the centralized optimization, before and after this sudden load change. Besides, with the help of the ASALVC, the voltage at bus 56 around $t = 20s$ closely tracks the optimal voltage at bus 56, determined by the centralized optimization, As there is a sudden load change, the ASALVC can be back to the optimal operating statuses with less time compared to the GPDC and SGPDC, indicating its stronger capability to quickly recover from such a sudden disturbance.

Next, we consider a more realistic and complex system with continuous fast system changes. The aggregate load and PV generation with continuous fast system changes, distributed across the modified IEEE 123-bus test system, are shown in Fig.7, where the time span is one day (24 hours) and the time granularity is 6 s. That is, the load and PV generation change rapidly every 6 seconds. Fig.8 shows the network voltage profiles with the ASALVC and without any control. As seen in Fig.8(a), there are voltage violations for the test system without any control around 18:00. However, it is observed from Fig.8(b) and Fig.9, despite the volatility in load and PV generation, the ASALVC can still effectively resolve voltage violation problems, not violating the capacity constraint.

TABLE III
VOLTAGE AND CAPACITY ISSUES UNDER THE DYNAMIC SCENARIO WITH CONTINUOUS FAST SYSTEM CHANGES

	CDC	DDC	GPDC	SGPDC	ASALVC
Voltage issue	Yes	Yes	No	No	No
Capacity issue	No	No	No	No	No

For comparison, other droop controls, including the CDC and DDC, GPDC, SGPDC, are taken into account to handle
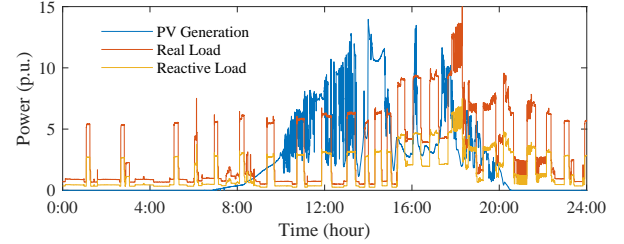

Fig. 7. Aggregate load and PV generation with continuous fast time-varying system changes.
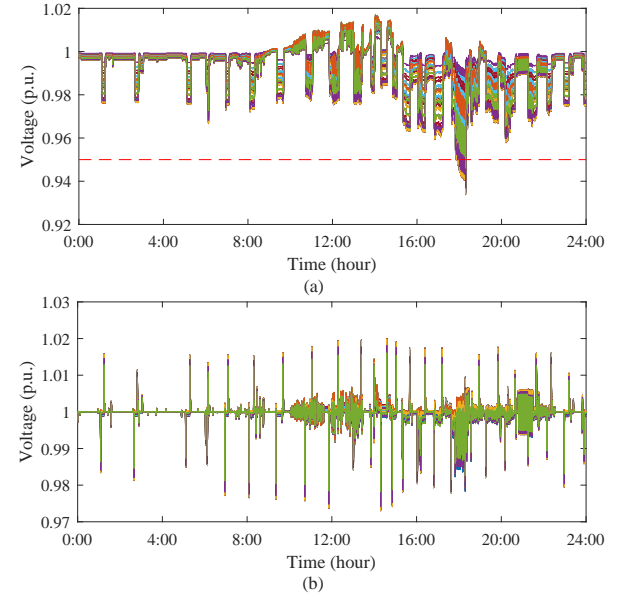

Fig. 8. The network voltage profile across the modified IEEE 123-bus test system (each curve depicts the voltage magnitude fluctuation for each bus): (a) Without any control; (b) With the ASALVC.

continuous fast system variations.[5] As shown in Table III, the CDC and DDC suffer from voltage violation problems under the dynamic scenario with continuous fast system changes. For the CDC, DDC, GPDC, SGPDC, and ASALVC, there are not capacity violation problems in the online implementation as the VAr limits can be updated online based on the given inverter capacities and the instantaneous real power of PV generators. The time average objective [6] across one day is selected as the metric to evaluate control performances. As shown in Fig.10, the performances of the CDC and DDC are poor under the dynamic scenario with continuous fast system changes. What explains this phenomenon? On the one hand, the CDC and DDC are associated with continuous slopes and intercepts, those droop control functions are not flexible to make full use of inverters' VAr outputs for voltage regulation. On the other hand, the CDC and DDC always suffer from stability and optimality problems, resulting in the poor performance in tracking

[5]Considering the centralized optimization is implemented after convergence, it is not suitable to apply the centralized optimization to the dynamic scenario with continuous fast system changes, thus the centralized optimization is not carried out here.

[6]The time average objective is the average objective value across time. The lower the time average objective is, the better its performance is.
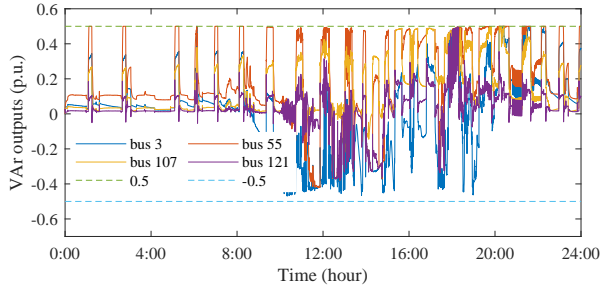
Fig. 9. VAr outputs of PV inverters at buses 3, 55, 107, 121 by using the ASALVC.
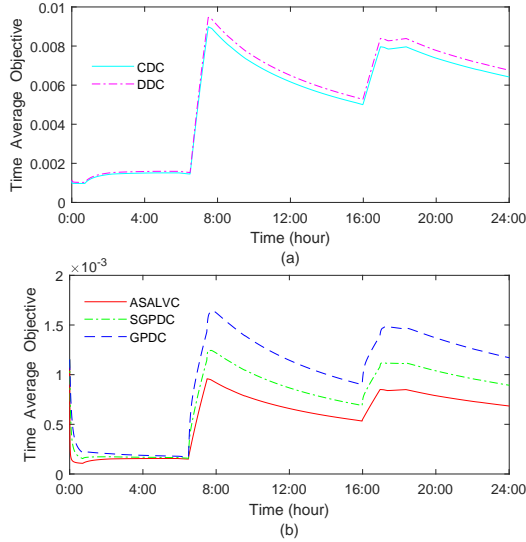

Fig. 10. Time average objectives for various VAr controls under the dynamic scenario with continuous fast system changes: (a) the performances of the CDC and DDC; (b) the performances of the GPDC, SGPDC, and ASALVC.

the continuous fast changes. Compared to the CDC and DDC, the GPDC, SGPDC, ASALVC show better performances due to the capability of considering the optimality property. As shown in Fig.10, the ASALVC still exhibits the best performance compared to the GPDC and SGPDC, indicating it is more capable of maintaining a flat network voltage profile even for the dynamic scenario with continuous fast system changes. As we discussed before, the ASALVC shows a faster convergence rate than other controls, leading to a greater tracking capability for continuous fast system changes in the dynamic scenario. In addition, the ASALVC is associated with both the time-varying slope and intercept, making itself more flexible to adapt to continuous fast system changes.

VI. CONCLUSION

This paper proposes an ASALVC strategy, where each bus agent locally adjusts the VAr output of its DER based on its time-varying voltage droop function. This voltage droop function is associated with the bus-specific time-varying slope and intercept, which can be dynamically updated merely based on the local voltage measurement. The dynamic adjustment characteristic enables the ASALVC to track time-varying system changes. Stability, convergence and optimality properties of

this local voltage control are analytically established. Through numerical case studies, it shows the ASALVC always exhibits the best performance compared to other controls in both static and dynamic scenarios, validating its effectiveness and superiority. Note that the proposed ASALVC can be further embedded into the two-layer VVC framework to consider discrete voltage regulation devices. In the upper layer, conventional discrete voltage regulation devices are scheduled over a slow timescale. In the lower layer, the VAr outputs of DERs can be modulated by our proposed ASALVC, where the setting of discrete voltage regulation devices is maintained at the upper-layer solution. Our future research will focus on meshed distribution networks and the data-driven learning-assisted implementation of local voltage control.

APPENDIX A

Proof of Proposition 1:

We introduce the function $z(\boldsymbol{x}) = \frac{1}{2}\boldsymbol{x}^T\boldsymbol{L}\boldsymbol{x} - f(\boldsymbol{x})$. Since $f(\boldsymbol{x})$ is continuously differentiable, we can know $z(\boldsymbol{x})$ is continuously differentiable. By exploiting [30, Theorem 2.1.3], it follows that $z(\boldsymbol{x})$ is convex if and only if $< \nabla z(\boldsymbol{q}^g) - \nabla z(\boldsymbol{y}), \boldsymbol{q}^g - \boldsymbol{y} > \geq 0$ holds for $\forall \boldsymbol{q}^g, \boldsymbol{y} \in \mathbb{R}^N$, which can be presented as follows:

$$
\begin{aligned}
&< \nabla z(\boldsymbol{q}^g) - \nabla z(\boldsymbol{y}), \boldsymbol{q}^g - \boldsymbol{y} >= \\
&- < \nabla f(\boldsymbol{q}^g) - \nabla f(\boldsymbol{y}), \boldsymbol{q}^g - \boldsymbol{y} > + ||\boldsymbol{q}^g - \boldsymbol{y}||_{\boldsymbol{L}}^2 \geq 0
\end{aligned} \tag{35}
$$

where (35) is equivalent to (12). Thus, (12) is the sufficient and necessary conditions for $z(\boldsymbol{x})$ is convex. From [31, Section 3.1.3], it follows that $z(\boldsymbol{x})$ is convex if and only if, for $\forall \boldsymbol{q}^g, \boldsymbol{y} \in \mathbb{R}^N$:

$$
\begin{aligned}
z(\boldsymbol{q}^g) &\geq z(\boldsymbol{y}) + \nabla z(\boldsymbol{y})^T(\boldsymbol{q}^g - \boldsymbol{y}) \\
&= \frac{1}{2}\boldsymbol{y}^T\boldsymbol{L}\boldsymbol{y} - f(\boldsymbol{y}) + < \boldsymbol{L}\boldsymbol{y} - \nabla f(\boldsymbol{y}), \boldsymbol{q}^g - \boldsymbol{y} > \\
&= -f(\boldsymbol{y}) - < \nabla f(\boldsymbol{y}), \boldsymbol{q}^g - \boldsymbol{y} > \\
&\quad - \frac{1}{2}||\boldsymbol{q}^g - \boldsymbol{y}||_{\boldsymbol{L}}^2 + \frac{1}{2}(\boldsymbol{q}^g)^T\boldsymbol{L}\boldsymbol{q}^g
\end{aligned} \tag{36}
$$

where (36) is equivalent to (11). Thus, (11) is also the sufficient and necessary conditions for $z(\boldsymbol{x})$ is convex. From the above analysis, it concludes this proof. Q.E.D.

APPENDIX B

Proof of Proposition 3:

It follows from Proposition 2 that (13) holds due to [P3.A]. As $g(\boldsymbol{q}^g)$ is an indicator function, we know $g(\boldsymbol{q}^g(k)) = g(\boldsymbol{q}^{g*}) = 0$. Then (11) boils down to:

$$
f(\boldsymbol{q}^g(k)) - f(\boldsymbol{q}^{g*}) \leq \frac{2||\boldsymbol{q}^g(0) - \boldsymbol{q}^{g*}||_{\boldsymbol{L}}^2}{(k+1)^2}, \forall k \geq 1 \tag{37}
$$

We introduce $z(\boldsymbol{x}) = f(\boldsymbol{x}) - \frac{1}{2}\boldsymbol{x}^T\boldsymbol{H}\boldsymbol{x}$. From [P3.B], we have:

$$
\begin{aligned}
&< \nabla z(\boldsymbol{q}^g) - \nabla z(\boldsymbol{y}), \boldsymbol{q}^g - \boldsymbol{y} > = \\
&< \nabla f(\boldsymbol{q}^g) - \nabla f(\boldsymbol{y}), \boldsymbol{q}^g - \boldsymbol{y} > - ||\boldsymbol{q}^g - \boldsymbol{y}||_{\boldsymbol{H}}^2 \\
&\quad\quad \geq ||\boldsymbol{q}^g - \boldsymbol{y}||_{\boldsymbol{H}}^2 - ||\boldsymbol{q}^g - \boldsymbol{y}||_{\boldsymbol{H}}^2 = 0
\end{aligned} \tag{38}
$$

By exploiting [30, Theorem 2.1.3], it follows from (38) that $z(\boldsymbol{x})$ is convex. For the convex function $z(\boldsymbol{x})$, for $\forall \boldsymbol{q}^g, \boldsymbol{y} \in \mathbb{R}^N$, it follows from [31, Section 3.1.3] that:

$$z(\boldsymbol{q}^g) \geq z(\boldsymbol{y}) + \nabla z(\boldsymbol{y})^T(\boldsymbol{q}^g - \boldsymbol{y}) \qquad (39)$$

It follows that:

$$f(\boldsymbol{q}^g) \geq f(\boldsymbol{y}) + <\nabla f(\boldsymbol{y}), \boldsymbol{q}^g - \boldsymbol{y}> + \frac{1}{2}||\boldsymbol{q}^g - \boldsymbol{y}||_H^2 \quad (40)$$

Then, we have:

$$f(\boldsymbol{q}^g(k)) \geq f(\boldsymbol{q}^{g*}) + <\nabla f(\boldsymbol{q}^{g*}), \boldsymbol{q}^g(k) - \boldsymbol{q}^{g*}> \\ + \frac{1}{2}||\boldsymbol{q}^g(k) - \boldsymbol{q}^{g*}||_H^2 \qquad (41)$$

From [31, Section 4.2.3], it follows that:

$$<\nabla f(\boldsymbol{q}^{g*}), \boldsymbol{q}^g(k) - \boldsymbol{q}^{g*}> \geq 0 \qquad (42)$$

Combining (41) and (42), we have:

$$f(\boldsymbol{q}^g(k)) - f(\boldsymbol{q}^{g*}) \geq \frac{1}{2}||\boldsymbol{q}^g(k) - \boldsymbol{q}^{g*}||_H^2 \qquad (43)$$

From (37) and (43), we have:

$$\frac{1}{2}||\boldsymbol{q}^g(k) - \boldsymbol{q}^{g*}||_H^2 \leq \frac{2||\boldsymbol{q}^g(0) - \boldsymbol{q}^{g*}||_L^2}{(k+1)^2}, \forall k \geq 1 \qquad (44)$$

Then, we obtain:

$$||\boldsymbol{q}^g(k) - \boldsymbol{q}^{g*}||_2^2 \leq \frac{4||\boldsymbol{q}^g(0) - \boldsymbol{q}^{g*}||_L^2}{(k+1)^2 \sigma_{\min}(\boldsymbol{H})}, \forall k \geq 1 \qquad (45)$$

Q.E.D.

APPENDIX C

Proof of Proposition 4:

$$m(\boldsymbol{q}^g(k)) - m(\hat{\boldsymbol{q}}^{g*}) \\ = m(\boldsymbol{q}^g(k)) - f(\boldsymbol{q}^{g*}) + f(\boldsymbol{q}^{g*}) - m(\hat{\boldsymbol{q}}^{g*}) \\ \leq m(\boldsymbol{q}^g(k)) - f(\boldsymbol{q}^{g*}) + \tau \\ = m(\boldsymbol{q}^g(k)) - f(\boldsymbol{q}^g(k)) + f(\boldsymbol{q}^g(k)) - f(\boldsymbol{q}^{g*}) + \tau \\ \leq m(\boldsymbol{q}^g(k)) - f(\boldsymbol{q}^g(k)) + \frac{2||\boldsymbol{q}^g(0) - \boldsymbol{q}^{g*}||_L^2}{(k+1)^2} + \tau \qquad (46)$$

where the first inequality follows by [P4.B], and the second inequality follows by [P4.C] and Proposition 2. With respect to $m(\boldsymbol{q}^g(k)) - f(\boldsymbol{q}^g(k))$, we have:

$$m(\boldsymbol{q}^g(k)) - f(\boldsymbol{q}^g(k)) \\ = \frac{1}{2}\big[||h(\boldsymbol{q}^g(k), \boldsymbol{d}) - \boldsymbol{V}_r||_\Phi^2 - ||h_l(\boldsymbol{q}^g(k), \boldsymbol{d}) - \boldsymbol{V}_r||_\Phi^2\big] \\ = \frac{1}{2}\big[||h(\boldsymbol{q}^g(k), \boldsymbol{d}) - h_l(\boldsymbol{q}^g(k), \boldsymbol{d}) + h_l(\boldsymbol{q}^g(k), \boldsymbol{d}) - \boldsymbol{V}_r||_\Phi^2 \\ - ||h_l(\boldsymbol{q}^g(k), \boldsymbol{d}) - \boldsymbol{V}_r||_\Phi^2\big] \\ \leq \frac{1}{2}\big[||h(\boldsymbol{q}^g(k), \boldsymbol{d}) - h_l(\boldsymbol{q}^g(k), \boldsymbol{d})||_\Phi^2 + ||h_l(\boldsymbol{q}^g(k), \boldsymbol{d}) - \boldsymbol{V}_r||_\Phi^2 \\ - ||h_l(\boldsymbol{q}^g(k), \boldsymbol{d}) - \boldsymbol{V}_r||_\Phi^2\big] \\ = \frac{1}{2}||h(\boldsymbol{q}^g(k), \boldsymbol{d}) - h_l(\boldsymbol{q}^g(k), \boldsymbol{d})||_\Phi^2 \qquad (47)$$

Since Φ is a symmetric positive definite matrix, it follows by Cholesky decomposition that Φ can be expressed by the form $\Phi = \boldsymbol{E}^T\boldsymbol{E}$. Then, we have:

$$||h(\boldsymbol{q}^g(k), \boldsymbol{d}) - h_l(\boldsymbol{q}^g(k), \boldsymbol{d})||_\Phi \\ = ||\boldsymbol{E}[h(\boldsymbol{q}^g(k), \boldsymbol{d}) - h_l(\boldsymbol{q}^g(k), \boldsymbol{d})]||_2 \\ \leq ||\boldsymbol{E}||_2||h(\boldsymbol{q}^g(k), \boldsymbol{d}) - h_l(\boldsymbol{q}^g(k), \boldsymbol{d})||_2 \\ = ||\boldsymbol{E}||_2\delta \qquad (48)$$

Combining (46)-(48), it follows that (20) holds. Q.E.D.

APPENDIX D

Proof of Proposition 5:

From (9)-(10), $\boldsymbol{q}^g(k) = p_{\boldsymbol{L}}(\boldsymbol{y}(k))$ can be represented by:

$$\boldsymbol{q}^g(k) = \underset{\underline{\boldsymbol{q}}^g \leq \boldsymbol{q}^g \leq \overline{\boldsymbol{q}}^g}{\arg\min} <\nabla f(\boldsymbol{y}(k)), \boldsymbol{q}^g - \boldsymbol{y}(k)> + \frac{1}{2}||\boldsymbol{q}^g - \boldsymbol{y}(k)||_L^2 \qquad (49)$$

For the diagonal positive definite matrix $\boldsymbol{L}$, (49) is equal to:

$$\boldsymbol{q}^g(k) = \underset{\underline{\boldsymbol{q}}^g \leq \boldsymbol{q}^g \leq \overline{\boldsymbol{q}}^g}{\arg\min} \sum_{i=1}^N \Big\{ \frac{\partial f(\boldsymbol{y}(k))}{\partial y_i(k)}[q_i^g - y_i(k)] + \frac{L_i}{2}[q_i^g - y_i(k)]^2 \Big\} \qquad (50)$$

It is clear that both the objective and constraint in (50) are decomposable, thus, for any $i \in \mathcal{N}.q_i^g(k)$ can be solved by:

$$q_i^g(k) = \underset{\underline{q}_i^g \leq q_i^g \leq \overline{q}_i^g}{\arg\min} \frac{\partial f(\boldsymbol{y}(k))}{\partial y_i(k)}[q_i^g - y_i(k)] + \frac{L_i}{2}[q_i^g - y_i(k)]^2 \qquad (51)$$

Note that $q_i^g(k)$ is a scalar, (51) is equivalently solved by (22). In this case, $\boldsymbol{q}^g(k)$ can be represented by (23). Q.E.D.

REFERENCES

[1] K. Turitsyn, P. Sulc, S. Backhaus and M. Chertkov, "Options for control of reactive power by distributed photovoltaic generators," *Proc. IEEE*, vol. 99, no. 6, pp. 1063-1073, June 2011.

[2] M. Farivar, R. Neal, C. Clarke and S. Low, "Optimal inverter VAR control in distribution systems with high PV penetration," in *2012 IEEE Power and Energy Society General Meeting*, 2012, pp. 1-7.

[3] S. Deshmukh, B. Natarajan and A. Pahwa, "Voltage/VAR control in distribution networks via reactive power injection through distributed generators," *IEEE Tran. Smart Grid*, vol. 3, no. 3, pp. 1226-1234. Sept. 2012.

[4] R. Cheng, Z. Wang, Y. Guo and F. Bu, "Analyzing photovoltaic's impact on conservation voltage reduction in distribution networks," in *2021 North American Power Symposium (NAPS)*, 2021, pp. 1-6.

[5] D. K. Molzahn, F. Dörfler, H. Sandberg, et al, "A survey of distributed optimization and control algorithms for electric power systems," *IEEE Trans. Smart Grid*, vol. 8, no. 6, pp. 2941-2962, Nov. 2017.

[6] X. Zhou, S. Zou, P. Wang and Z. Ma, "Voltage regulation in constrained distribution networks by coordinating electric vehicle charging based on hierarchical ADMM", *IET Generation Transmission & Distribution*, vol. 14, pp. 3444-3457, 2020.

[7] Y. Guo, H. Gao, H. Xing, Q. Wu and Z. Lin, "Decentralized coordinated voltage control for VSC-HVDC connected wind farms based on ADMM," *IEEE Trans. Sustain. Energy*, vol. 10, no. 2, pp. 800-810, April 2019.

[8] E. Dall'Anese, S.V. Dhople, B.B. Johnson and G.B. Giannakis, "Decentralized optimal dispatch of photovoltaic inverters in residential distribution systems," *IEEE Transactions on Energy Conversion*, vol. 29, no. 4, pp. 957-967, Dec. 2014.

[9] R. Cheng, Z. Wang, Y. Guo, "Online voltage control for unbalanced distribution networks using projected newton method," *IEEE Trans. Power Syst.*, in press, 2021.

[10] B.A. Robbins and A.D. Domínguez-García, "Optimal reactive power dispatch for voltage regulation in unbalanced distribution systems," *IEEE Trans. Power Syst.*, vol. 31, no. 4, pp. 2903-2913, Jul. 2016.

[11] P. Šulc, S. Backhaus, and M. Chertkov, "Optimal distributed control of reactive power via the alternating direction method of multipliers," *IEEE Trans. Energy Convers.*, vol. 29, no. 4, pp. 968–977, Dec. 2014.

[12] H.J. Liu, W. Shi, and H. Zhu, "Distributed voltage control in distribution networks: online and robust implementations," *IEEE Trans. Smart Grid*, vol. 9, no. 6, pp. 6106–6117, Nov. 2018.

[13] Z. Tang, D.J. Hill and T. Liu, "Fast distributed reactive power control for voltage regulation in distribution networks," *IEEE Trans. Power Syst.*, vol. 34, no. 1, pp. 802-805, Jan. 2019.

[14] G. Qu and N. Li, "Optimal distributed feedback voltage control under limited reactive power," *IEEE Trans. Power Syst.*, vol. 35, no. 1, pp. 315-331, Jan. 2020.

[15] R. Neal and R. Bravo, "Advanced Volt/VAr control element of Southern California Edison's Irvine smart grid demonstration," in *Proc. IEEE Power Syst. Conf. Expo. (PSCE)*, Phoenix, AZ, USA, Mar. 2011, pp. 1–3.

[16] M. Farivar, L. Chen, and S. Low, "Equilibrium and dynamics of local voltage control in distribution systems," in *Proc. 52nd IEEE Conf. Decis. Control*, 2013, pp. 4329–4334.

[17] *IEEE standard for interconnection and interoperability of distributed energy resources with associated electric power systems interfaces*, IEEE Standard 1547-2018, Feb. 15, 2018.

[18] N. Li, G. Qu and M. Dahleh, "Real-time decentralized voltage control in distribution networks," in *Proc. 52nd Annual Allerton Conference on Communication, Control, and Computing (Allerton)*, 2014, pp. 582-588.

[19] P. Jahangiri and D. C. Aliprantis, "Distributed Volt/VAr control by PV inverters", *IEEE Trans. Power Syst.*, vol. 28, no. 3, pp. 3429-3439, Aug. 2013.

[20] F. Andrén, B. Bletterie, S. Kadam, P. Kotsampopoulos and C. Bucher, "On the stability of local voltage control in distribution networks with a high penetration of inverter-based generation," *IEEE Transactions on Industrial Electronics*, vol. 62, no. 4, pp. 2519-2529, April 2015.

[21] G. Cavraro and R. Carli, "Local and distributed voltage control algorithms in distribution networks," *IEEE Trans. Power Syst.*, vol. 33, no. 2, pp. 1420-1430, March 2018.

[22] Y. Guo, H. Gao, D. Wang and Q. Wu, "Online optimal feedback voltage control of wind farms: decentralized and asynchronous implementations," *IEEE Trans. Sustain. Energy*, vol. 12, no. 2, pp. 1489-1492, April 2021.

[23] H. Zhu and H.J. Liu, "Fast local voltage control under limited reactive power: optimality and stability analysis," *IEEE Trans. Power Syst.*, vol. 31, no. 5, pp. 3794-3803, Sep. 2016.

[24] D. P. Bertsekas, *Nonlinear Programming*, Second Edition, Athena Scientific, Belmont, MA, USA, 1999.

[25] D. P. Bertsekas, "On the Goldstein-Levitin-Polyak gradient projection method," *IEEE Transactions on Automatic Control*, vol. 21, no. 2, pp. 174-184, April 1976.

[26] A. Beck and M. Teboulle, "A fast iterative shrinkage-thresholding algorithm for linear inverse problems," *SIAM J. Imag. Sci.*, vol. 2, no. 1, pp. 183–202, Mar. 2009.

[27] W. Zuo and Z. Lin, "A generalized accelerated proximal gradient approach for total-variation-based image restoration," *IEEE Transactions on Image Processing*, vol. 20, no. 10, pp. 2748-2759, Oct. 2011.

[28] M.E. Baran and F.F. Wu, "Optimal capacitor placement on radial distribution systems," *IEEE Trans. Power Del.*, vol. 4, no. 1, pp. 725-734, Jan. 1989.

[29] R. Cheng, L. Tesfatsion, Z. Wang, "A multiperiod consensus-based transactive energy system for unbalanced distribution networks," ISU Digital Repository, Iowa State Univ., Ames, IA, USA, 2021. [Online]. Available: https://dr.lib.iastate.edu/handle/20.500.12876/104714

[30] Y. Nesterov, *Introductory lectures on convex optimization: A basic course*, Springer Science & Business Media, 2003.

[31] S. Boyd and L. Vandenberghe, *Convex Optimization*, Seventh Printing, Cambridge University Press, Cambridge, UK, 2009.

[32] R.D. Zimmerman, C.E.Murillo-Sánchez and R.J.Thomas, "MAT-POWER: Steady-State operations, planning, and analysis tools for power systems research and education," *IEEE Trans. Power Syst.*, vol. 26, no. 1, pp. 12-19, Feb. 2011.

[33] C. Bliek, P. Bonami, and A. Lodi, "Solving mixed-integer quadratic programming problems with IBM-CPLEX: a progress report," in *Proc. 26th RAMP Symposium*, Tokyo, Japan, Oct. 2014.